International Journal of Mechanical Sciences 52 (2010) 1547–1562

Contents lists available at ScienceDirect

International Journal of Mechanical Sciences

journal homepage: www.elsevier.com/locate/ijmecsci

Nonlinear dynamic behavior and instability of slender frames with semi-rigid connections

Alexandre S. Galvão [a], Andréa R.D. Silva [b], Ricardo A.M. Silveira [b], Paulo B. Gonçalves [c,*]

[a] Universidade Federal Fluminense, Campus of Volta Redonda, Av. dos Trabalhadores, Vila Santa Cecília, 27260-270 Volta Redonda, RJ, Brazil
[b] Department of Civil Engineering, School of Mines, Federal University of Ouro Preto, Campus Universitário s/n, Morro do Cruzeiro, 35400-000 Ouro Preto, MG, Brazil
[c] Department of Civil Engineering, Pontifical Catholic University, PUC-Rio, Rua Marquês de São Vicente, 225, Gávea, 22453-900 Rio de Janeiro, RJ, Brazil

ARTICLE INFO

Article history:
Received 27 August 2009
Received in revised form
4 June 2010
Accepted 12 July 2010
Available online 14 July 2010

Keywords:
Structural stability
Nonlinear dynamic analysis
Vibration analysis of pre-loaded structures
Semi-rigid connections
Frames

ABSTRACT

The free and forced nonlinear vibrations of slender frames with semi-rigid connections are studied in this work. Special attention is given to the influence of static pre-load on the natural frequencies and mode shapes, nonlinear frequency–amplitude relations, and resonance curves. An efficient nonlinear finite element program for buckling and vibration analysis of slender elastic frames with semi-rigid connections is developed. The equilibrium paths are obtained by continuation techniques, in combination with the Newton-Raphson method. The ordinary differential equations of motion of the discretized frame are solved by the Newmark implicit numerical integration method using adaptive time-step strategies. Three structural systems with important practical applications are analyzed: an *L*-frame, a shallow arch, and a pitched-roof frame. The results highlight the importance of the static pre-load and the stiffness of the semi-rigid connections on the buckling and vibration characteristics of these structures.

1. Introduction

Recent advances in structural engineering incorporating new or enhanced materials, together with improved mathematical modeling and more precise numerical computational tools, with models that permit realistic simulation and resolution of structural problems, have led to more efficient and slender structural members. This is particularly true in structures where their weight effects must be minimized, such as aerospace structures, large span civil engineering constructions, and off-shore structures. However, the increasing slenderness of structural elements makes them more susceptible to vibration and buckling problems. Additionally, this increases the influence of nonlinearities, particularly geometric nonlinearities, on their static and dynamic behavior. These effects are usually exacerbated by the presence of static pre-load as well as geometric and load imperfections. The interaction of these factors is particularly important in the analysis of structures predisposed to buckling. Therefore, a precise nonlinear analysis is essential for a safe design of this class of structures.

In most reports on linear and nonlinear structure vibrations, it is assumed that the system is free of loading and that a dynamic load is suddenly applied for a given time duration. This may lead to erroneous results when slender structures susceptible to buckling are investigated. Simitses [1,2] discussed the effects of static preloading on the dynamic stability of structures. His works deal with systems that are first loaded quasistatically to a level below the static critical load and subsequently subjected to dynamic loads. The effect of static pre-load on the structure dynamics has also been studied by Wu and Thompson [3], Machado and Cortínez [4], and Zeinoddini et al. [5], among others. The interplay between buckling and vibration has been the subject of several previous papers [5–13]. Other investigations have dealt with the vibration characteristics of buckled structures [14–17].

These studies show that compressive stress states decrease the structure natural frequencies and may even change the mode shapes associated with the lowest natural frequencies [6]. They also decrease the effective stiffness and consequently increase the vibration amplitudes, which may weaken or even damage the structure. Finally, shifting the natural frequencies to a lower frequency range may increase resonance problems due to environmental loads. Solutions to these vibration problems usually require the use of costly control systems or changes in the structural design [18].

It is well known that, in many frame structures, analyzing columns or beam-columns as independent members may cause erroneous results, particularly for large deflections [19]. In some configurations, the critical load and post-buckling behavior is

* Corresponding author. Fax: +55 21 3527 1195.
E-mail addresses: asgalvao@vm.uff.br (A.S. Galvão), andreadiassilva@yahoo.com.br (A.R. Silva), ricardo@em.ufop.br (R.A. Silveira), paulo@puc-rio.br (P.B. Gonçalves).

0020-7403/$ - see front matter © 2010 Elsevier Ltd. All rights reserved.
doi:10.1016/j.ijmecsci.2010.07.002

affected by other members connected to the columns. Because of this, the buckling and post-buckling analysis of frames is an important problem in structural design, particularly for slender frame analysis. While columns exhibit stable symmetric bifurcations with small post-buckling curvature, frames may exhibit stable, unstable, and asymmetric bifurcations [20–23]. The influence of the frame parameters, boundary conditions, and load and geometric imperfections on the equilibrium and stability behavior of *L*-frames was analyzed by Galvão et al. [24]. This geometry has also been used by several authors to test the efficiency of several nonlinear finite element formulations for planar frames, as well as incremental-iterative strategies for the solution of eminently nonlinear problems, due to the highly nonlinear response of *L*-frames under eccentric loads [25]. An important practical frame geometry is the so-called pitched-roof frame. Recently, the nonlinear post-buckling behavior of pitched-roof frames was extensively investigated by Silvestre and Camotim [22,23]. The authors examined several aspects of the nonlinear behavior and stability of this structure, taking into consideration that, in general, the elastic in-plane buckling behavior of pitched-roof frames is conditioned by global symmetric and anti-symmetric configuration modes. Although most frames lose stability at a bifurcation point, some shallow frames, such as the Williams frame [26], may lose stability at a limit point with a nonlinear behavior similar to that of a shallow arch. Therefore, in this work, three structures are analyzed to cover the characteristic behaviors: an *L*-frame, a shallow arch, and a pitched-roof frame.

The influence of the type of column–beam connection is also important in the calculation of buckling loads, natural frequencies, mode shapes, and nonlinear frame behavior [27]. In most publications, frames are assumed to be connected either by rigid or pinned joints. However, strictly speaking, all joints are semi-rigid, so this assumption does not normally represent the actual behavior of a realistic frame. The influence of semi-rigid connections on the buckling and post-buckling behavior of metal frames and the characterization of realistic connections is an important research area [28–31].

The dynamic behavior of structures with semi-rigid joints has not been extensively investigated. The influence of semi-rigid connections and mode shapes of frames was studied by Kawashima and Fujimoto [32], Chan [33], and Sophianopoulos [34], among others. Transient linear and nonlinear analysis of beams and frames with semi-rigid connections, as well as the study of vibratory problems associated with these structural systems, can also be found in publications by Chan [33], Shi and Atluri [35], Chan and Ho [36], Chui and Chan [37,38], Chan and Chui [39], Sekulovic et al. [40], and da Silva et al. [41].

The aim of the present work is to conduct a dynamic analysis of slender frames and to study the influence of second-order effects generated by large displacements and rotations, connection flexibility, initial geometric and load imperfections, and prestress states on the nonlinear response of the structures. An efficient nonlinear finite element program that includes the influence of connection stiffness, static pre-load as well as load, and geometric imperfections is developed for the static and dynamic structural analysis of planar elastic frames. The use of continuation techniques enables one to obtain the highly nonlinear equilibrium paths exhibited by the chosen examples, identify the bifurcation and limit points along these equilibrium

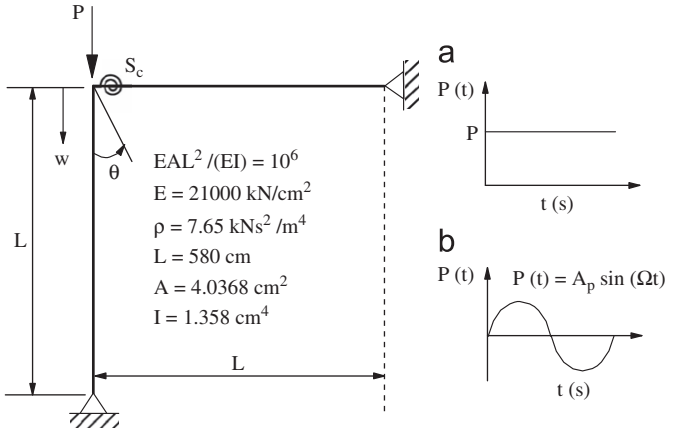

Fig. 1. *L*-frame with semi-rigid connection and dynamic loading.

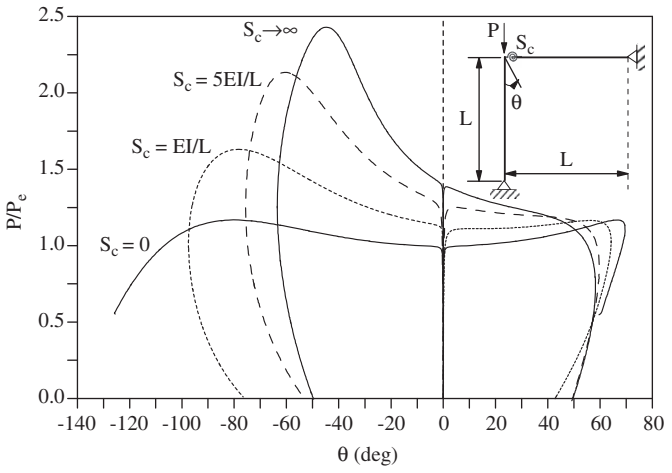

Fig. 2. Influence of the stiffness of the semi-rigid connection *Sc* on the *L*-frame post-buckling behavior.

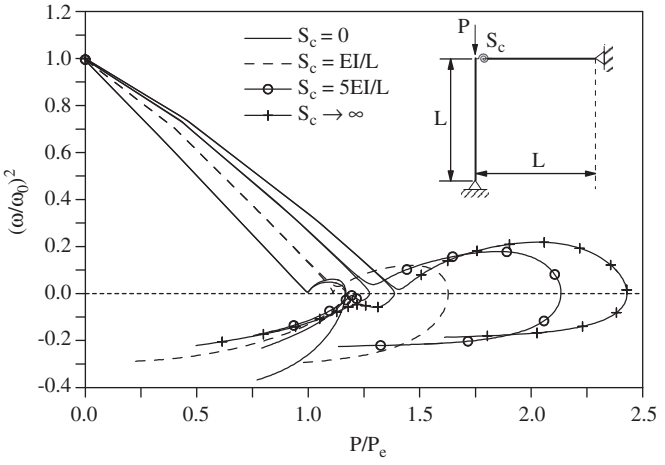

Fig. 3. Influence of the stiffness of the semi-rigid connection S_c on the natural frequency–load relation.

Table 1
Unloaded *L*-frame: first three natural frequencies versus stiffness parameter S_c.

S_c	ω_1	ω_2	ω_3
0	8.915	8.915	35.665
EI/L	8.915	10.238	35.665
5EI/L	8.915	12.131	35.665
∞	8.915	13.928	35.665

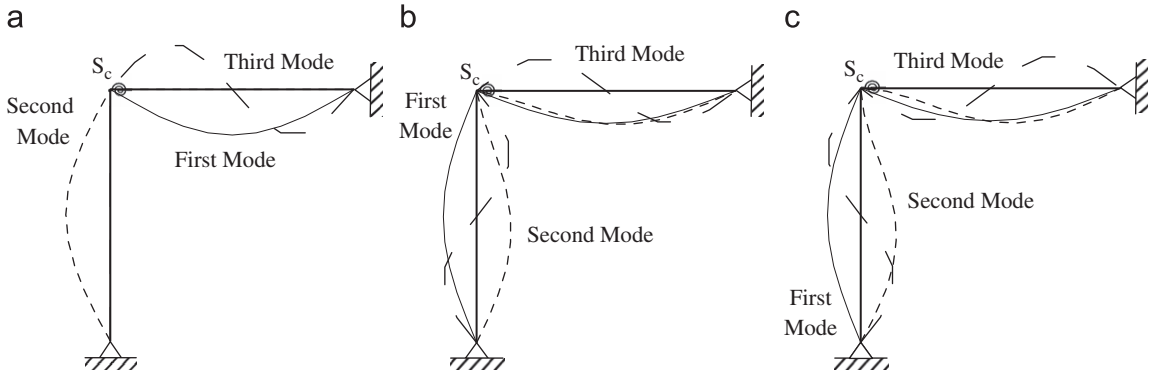

Fig. 4. Free vibration modes for selected values of the connection stiffness S_c. (a) $S_c=0$, (b) $S_c=5EI/L$ and (c) $S_c\to\infty$.

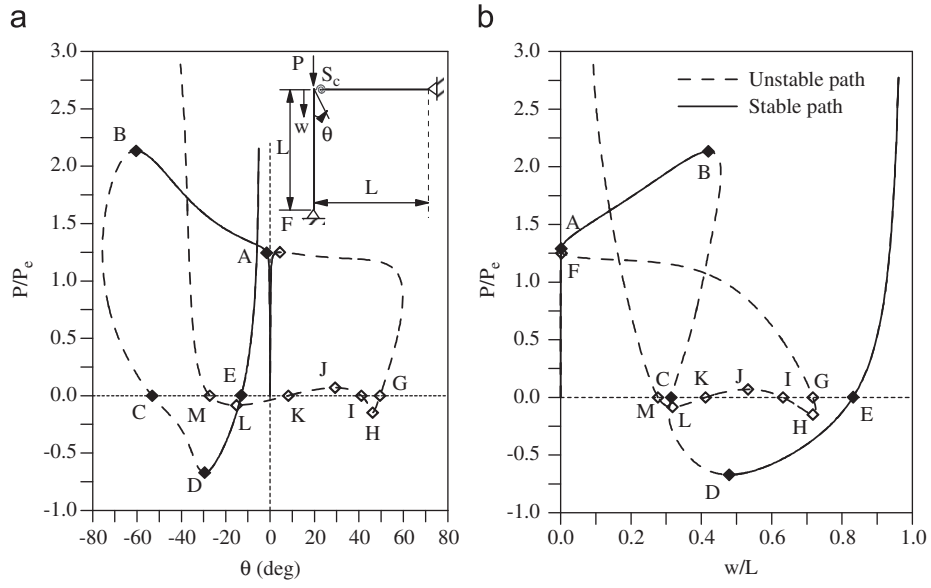

Fig. 5. Nonlinear equilibrium paths of the L-frame for $S_c=5EI/L$. (a) Rotation θ and (b) displacement w.

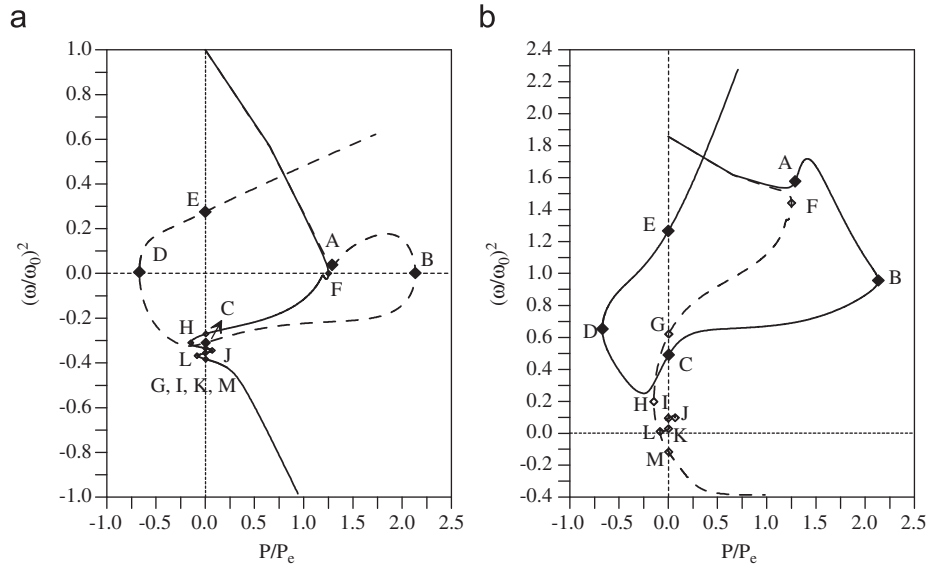

Fig. 6. Frequency–load relations of the L-frame for $S_c=5EI/L$. (a) First natural frequency–load relation and (b) second natural frequency-load relation.

paths, and calculate the vibration frequencies and modes along these paths. Therefore, one can identify the stable and unstable branches of these paths and study how the modes and frequencies vary as a function of static pre-loading. The Newmark method together with a variable time increment adaptive strategy is used in the nonlinear free and forced vibration analysis. The geometric nonlinear finite element formulation for frames with rigid connections implemented here is based on work by Alves [42], Yang and Kuo [43], and Galvão [44]. The consideration of semi-rigid connections is based on the finite element formulation proposed by Chan and Chui [39].

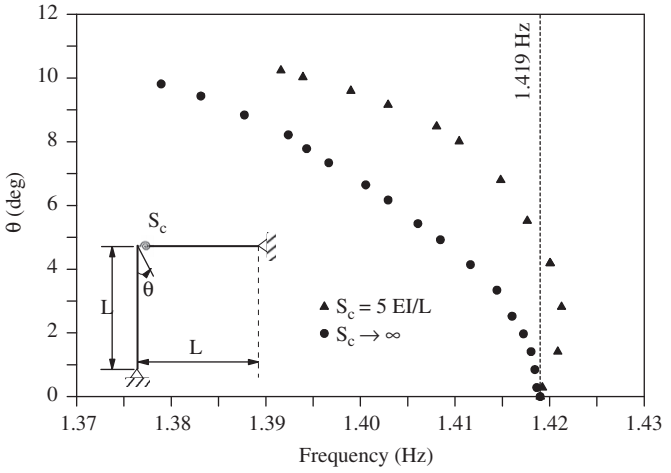

Fig. 7. Nonlinear frequency–amplitude relation for selected values of the connection stiffness S_c.

2. The nonlinear static equilibrium and free vibration problems

In the finite element method context, the equilibrium of any structural system can be expressed as

$$\boldsymbol{F}_i(\boldsymbol{u}) = \lambda \boldsymbol{F}_r \tag{1}$$

where $\boldsymbol{F}_i$ is the internal forces vector, function of the generalized displacement vector $\boldsymbol{u}$, λ is a load factor, and $\boldsymbol{F}_r$ is a fixed reference vector defining the direction and distribution of the applied load.

To obtain the nonlinear equilibrium path of a structure, an incremental technique for the response is used to solve the system of equations (1). This procedure basically consists of calculating a sequence of incremental displacements, $\Delta \boldsymbol{u}_i$, that correspond to a sequence of given load increments $\Delta\lambda_i$. However, as $\boldsymbol{F}_i$ is a nonlinear function of the displacements, the estimated solution for the problem (predicted solution: $\Delta\lambda^0$, $\Delta\boldsymbol{u}^0$) for each load step normally does not satisfy Eq. (1). Consequently, a residual force vector $\boldsymbol{g}$ is defined

$$\boldsymbol{g} = \lambda \boldsymbol{F}_r - \boldsymbol{F}_i(\boldsymbol{u}) \tag{2}$$

If the unbalanced forces represented by $\boldsymbol{g}$ do not satisfy the convergence criteria, a new estimate for the displacements is

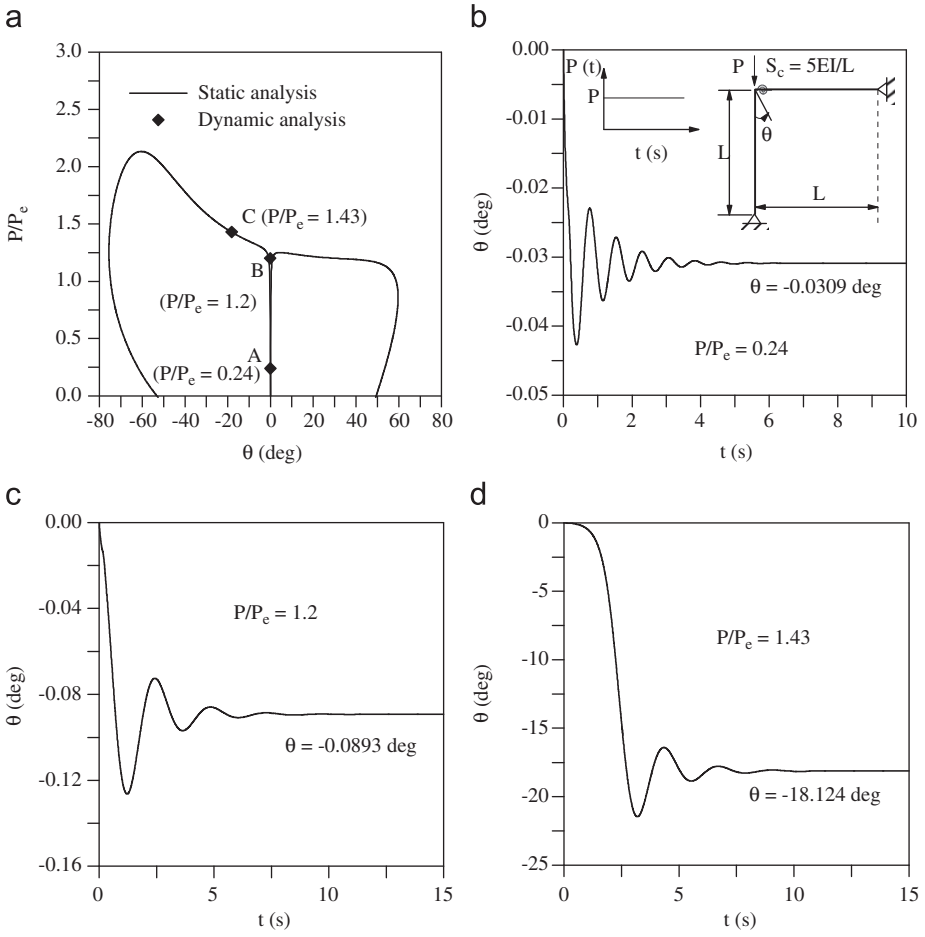

Fig. 8. Static and dynamic responses of the *L*-frame submitted to increasing load levels. Step load of infinite duration. (a) Nonlinear static analysis, (b) point A in (a), (c) point B in (a), (d) point C in (a).

obtained by the relation

$$\boldsymbol{K}_t \delta \boldsymbol{u} = \boldsymbol{g} \tag{3}$$

where $\boldsymbol{K}_t$ is the tangent stiffness matrix of the structural system and $\delta \boldsymbol{u}$ is the residual displacement vector.

The estimate of the correction $\Delta \boldsymbol{u}$ is not directly obtained by solving Eq. (3). Instead, the residual displacement vector is defined as a sum of two components [43,44]:

$$\delta \boldsymbol{u} = \delta \boldsymbol{u}_g + \delta\lambda \delta \boldsymbol{u}_r \tag{4}$$

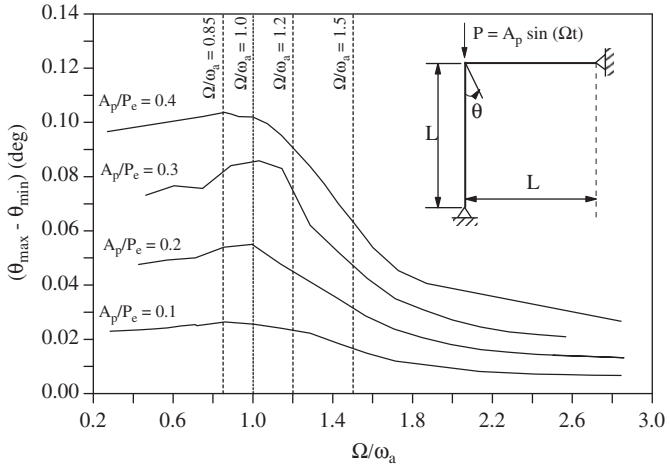

Fig. 9. Resonance curves for the *L*-frame with rigid connections submitted to a harmonic load concentrated on the top of the column.

where $\delta\lambda$ is a load parameter that, to make the correction process more efficient, is evaluated in an iterative cycle that also corrects the load increment, and $\delta \boldsymbol{u}_g$ and $\delta \boldsymbol{u}_r$ are obtained by

$$\delta \boldsymbol{u}_g = \boldsymbol{K}_t^{-1} \boldsymbol{g} \tag{5a}$$

$$\delta \boldsymbol{u}_r = \boldsymbol{K}_t^{-1} \boldsymbol{F}_r \tag{5b}$$

These displacement vectors can be easily obtained since $\boldsymbol{K}_t$, $\boldsymbol{g}$, and $\boldsymbol{F}_r$ are known. The definition of $\delta\lambda$ in Eq. (4) depends on a constraint equation to be added to the nonlinear problem (for example, an arc-length constraint equation).

The vibration frequencies and the corresponding modes of vibration in a loaded structure can be obtained by solving the following eigenvalue problem:

$$[(\boldsymbol{K}_L + \boldsymbol{K}_\tau) - \omega^2 \boldsymbol{M}]\boldsymbol{X} = \boldsymbol{0} \tag{6}$$

where $\boldsymbol{K}_L$ and $\boldsymbol{K}_\tau$ are the linear and geometric stiffness matrices, respectively, $\boldsymbol{M}$ is the mass matrix, which also considers the effect of the semi-rigid connection, ω is the natural frequency, and $\boldsymbol{X}$ is the vibration mode vector. Appendix A illustrates the step-by-step numerical procedures for solving the static nonlinear problem and, subsequently, calculating the natural frequencies and vibration modes.

2.1. Semi-rigid connections

In this work, the consideration of semi-rigid connections is based on the finite element formulation proposed by Chan and Chui [39], where the connection is represented as a rotational linear spring with stiffness $S_c = kEI/L$. In the elastic global analysis

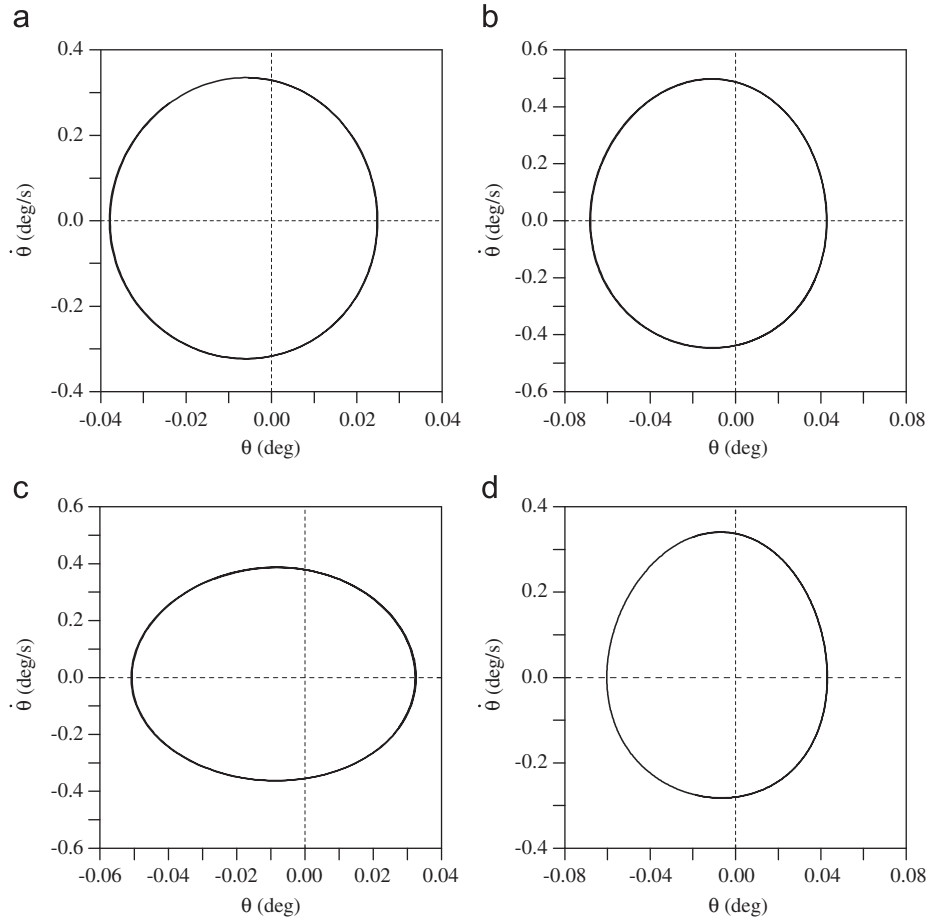

Fig. 10. Phase planes for $A_p/P_e = 0.4$. (a) $\Omega/\omega_a = 1.5$, (b) $\Omega/\omega_a = 1.2$, (c) $\Omega/\omega_a = 1.0$ and (d) $\Omega/\omega_a = 0.85$.

of frames the joints are usually classified in some design codes according to their rotational stiffness S_c as nominally pinned, rigid and semi-rigid. For example, according to Eurocode 3 [50], the stiffness of the beam-to-column connections, $S_c = k_b EI_b/L_b$, can be classified as:

- Nominally pinned, for $k_b \leq 0.5$.
- Semi-rigid, for $0.5 < k_b \leq \bar{k}_b$.
- Rigid, for $k_b \geq \bar{k}_b$.

where $\bar{k}_b = 8$ for braced frames where the bracing system reduces the horizontal displacement by at least 80% and $\bar{k}_b = 25$ for other frames provided that in every storey $k_b/k_c \geq 0.1$. Here the subscript b refers to beam and c to column.

3. The nonlinear transient problem

In the finite element context, the nonlinear time response of the structure can be obtained by solving the following set of discrete equations of motion:

$$\boldsymbol{M}\ddot{\boldsymbol{u}} + \boldsymbol{C}\dot{\boldsymbol{u}} + \boldsymbol{F}_i(\boldsymbol{u}) = \lambda(t)\boldsymbol{F}_r \tag{7}$$

where $\boldsymbol{M}$ and $\boldsymbol{C}$ are the mass and viscous damping matrices, respectively, and $\boldsymbol{F}_i$ is the internal force vector that depends on the displacement vector $\boldsymbol{u}$ of the system, $\dot{\boldsymbol{u}}$ and $\ddot{\boldsymbol{u}}$ are the velocity and acceleration vectors, respectively, and $[\lambda(t)\boldsymbol{F}_r]$ is the external excitation vector.

The solution of the nonlinear dynamic system (7) can be obtained through a time integration algorithm together with adaptive strategies for the automatic increment of the time step. The numerical methodology used here is presented in Appendix B.

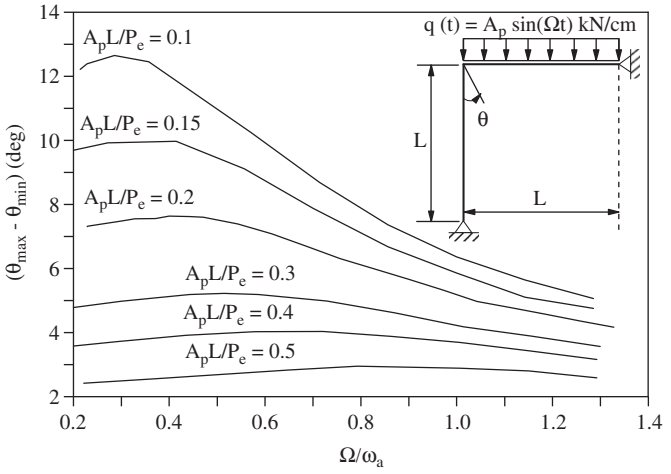

Fig. 11. Resonance curves for an *L*-frame under distributed load.

The numerical integration algorithm is based on the work by Dokainish and Subbaraj [45], while the time increment strategy is based on work by Jacob [46]. Details of the nonlinear dynamic formulation as well as the computational program are found in Galvão [44].

3.1. Nonlinear vibration analysis

The nonlinear frequency–amplitude relation provides fundamental information on the nonlinear vibration analysis of any structural system, and it gives a good indication of the type

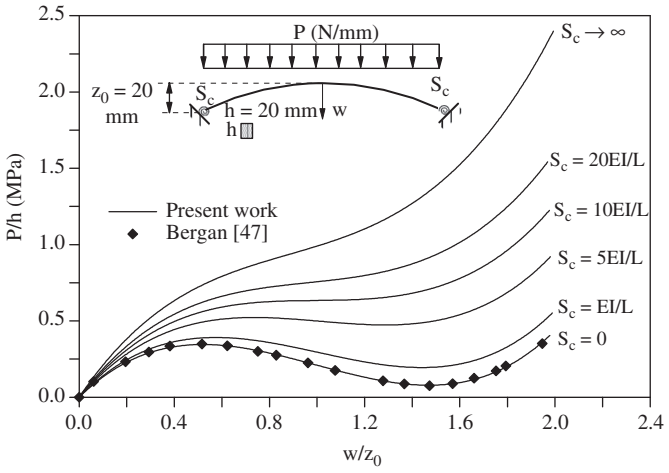

Fig. 13. Arch nonlinear equilibrium paths for different joint stiffness values S_c.

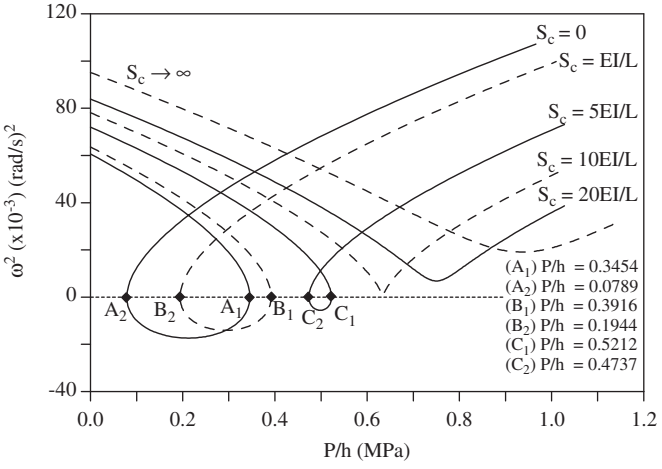

Fig. 14. Influence of the static pre-load on the lowest natural frequency of a shallow arch for different joint stiffness values S_c.

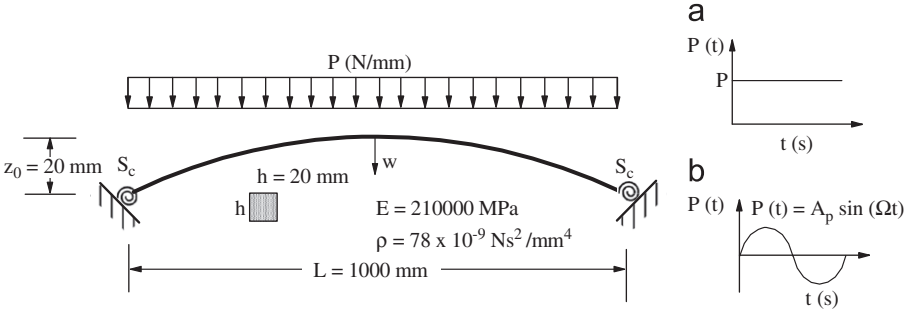

Fig. 12. Arch with semi-rigid joints under static and dynamic loading.

(hardening or softening) and degree of nonlinearity of the system. Various approaches, including perturbation methods and the harmonic balance method, have been developed to study nonlinear oscillators with a small number of degrees of freedom. Here the methodology proposed by Nandakumar and Chatterjee [48] is used to obtain this relation using the finite element method. First, the nonlinear equations of motion are numerically integrated, and the time response of the slightly damped system is obtained for a chosen node. Then, the maximum amplitude and corresponding period between two consecutive positive peaks are computed at each cycle. Consider two successive peaks at times T_1 and T_2. Let their average value be A_1 and let the trough between these two positive peaks be A_2. We then define the amplitude as $A=(A_1-A_2)/2$ and the frequency as $f=1/(T_1-T_2)$. The resulting amplitude and frequency values are plotted to give the frequency–amplitude relation. To obtain the peak amplitudes with the necessary accuracy, a small time step must be imposed in the integration process. In addition, a large number of elements are necessary to describe accurately the large amplitude response of the structure.

Low-dimensional numerical models employ relatively easy techniques for obtaining nonlinear resonance curves. In contrast, it is extremely computationally difficult to obtain these curves for structural systems with a large number of degrees of freedom. Here, a simple repetitive procedure coupled with the integration method is implemented, which consists of giving constant excitation–frequency increments $\Delta\Omega$ and, for each incremental step, integrating the differential equations of motion during N harmonic excitation cycles. The response of the initial cycles associated with the short transient response is dismissed, and the maximum amplitude of the steady-state solution is plotted as a function of the forcing frequency. Of course, this brute force method is unable to obtain unstable branches of resonance curves. In the developed program, the N and $\Delta\Omega$ parameters are

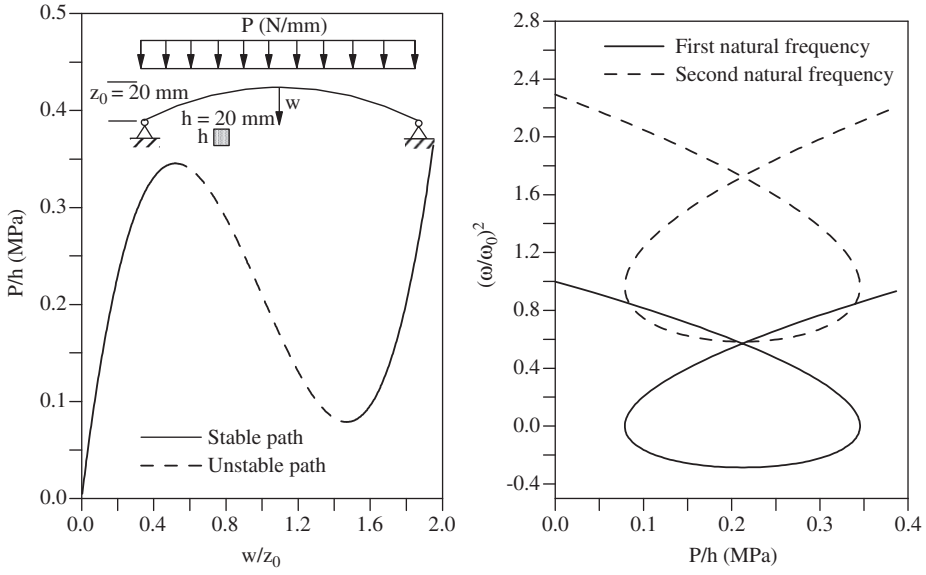

Fig. 15. Arch equilibrium paths and natural frequency–load relation for $z_0=20$ mm.

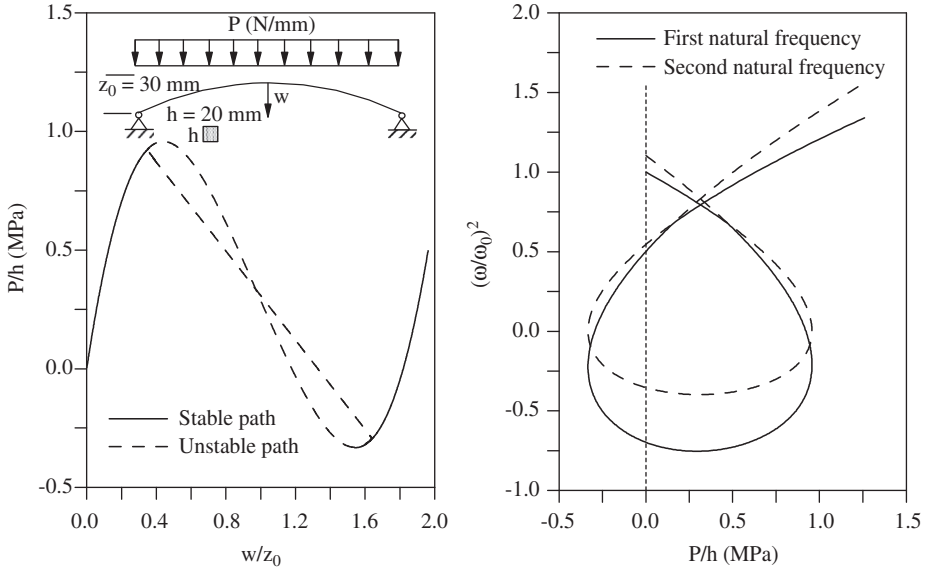

Fig. 16. Arch equilibrium paths and natural frequency–load relation for $z_0=30$ mm.

defined by the user, together with the integration method to be used, and then an adaptive strategy for the variable time increment is applied [46].

4. Numerical examples

Three structural problems are used to test the formulation and to show the possible buckling and vibration characteristics of slender frames: an *L*-frame, a shallow arch, and a pitched-roof frame. The free vibration analyses involve the calculation of the natural frequencies and vibration modes and the load–frequency relation. This study is fundamental for understanding the process of stability loss in structures with a high degree of nonlinearity and complicated equilibrium paths. Their nonlinear behavior under dynamic loads is also verified.

4.1. L-frame

In Galvão et al. [24], a detailed parametric analysis of the elastic stability of *L*-frames was performed. The geometrical and physical properties of the frame are presented in Fig. 1.

4.1.1. Instability and vibration analysis

L-frames usually display an asymmetric bifurcation, characterized by an initial non-zero slope of the post-critical equilibrium path. Galvão et al. [24] observed that, when the stiffness of the beam–column connection increases, the frame's critical load increases, and the initial slope of the asymmetric post-critical path simultaneously increases, resulting in the structure becoming more sensitive to initial imperfections. This characteristic is shown in Fig. 2, where the variation of the load parameter P/P_e is plotted as a function of the node rotation, θ, for different values of the connection stiffness parameter S_c. P_e is the Euler critical load. Small perturbations are used in the numerical strategy to obtain the two branches of the post-critical path. As $S_c \to 0$, the influence of the lateral bracing decreases, and the post-buckling path approaches that of a simply supported column (pinned connection).

The nonlinear relation between the load parameter and the natural frequencies for different values of joint stiffness is given in Fig. 3. This relation not only shows the influence of the static

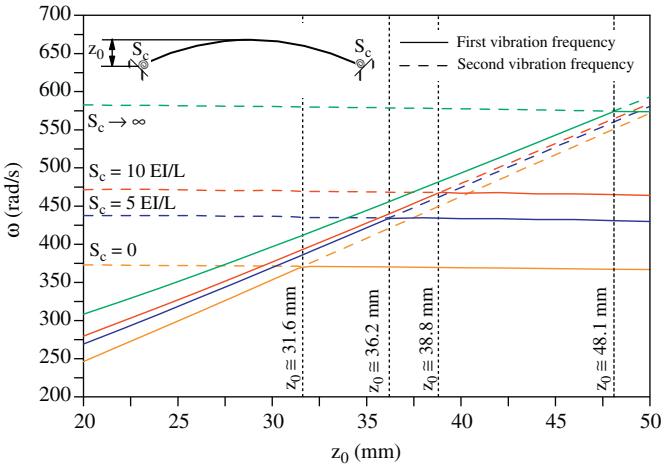

Fig. 19. Variation of two smallest natural frequencies with the arch height (z_0) for selected values of the support stiffness S_c.

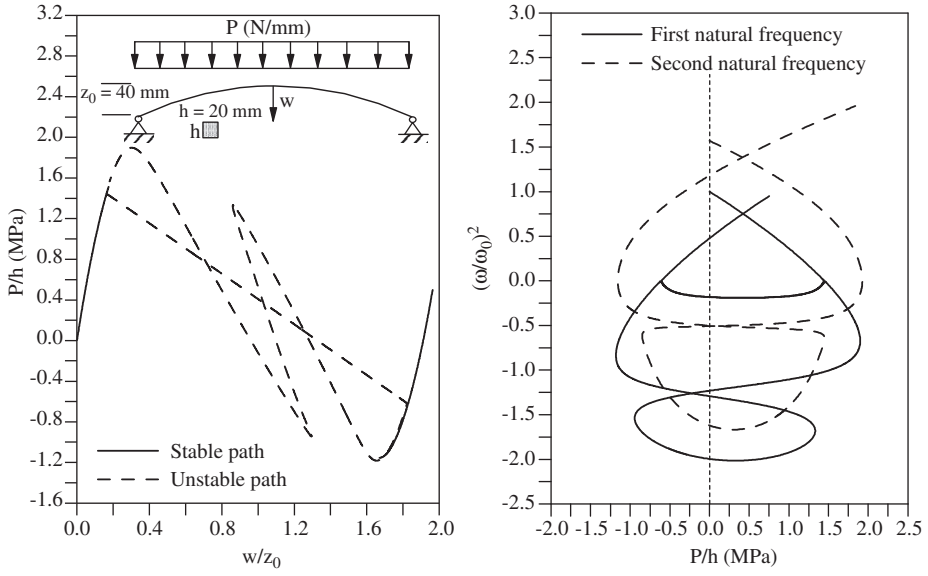

Fig. 17. Arch equilibrium paths and natural frequency–load relation for z_0=40 mm.

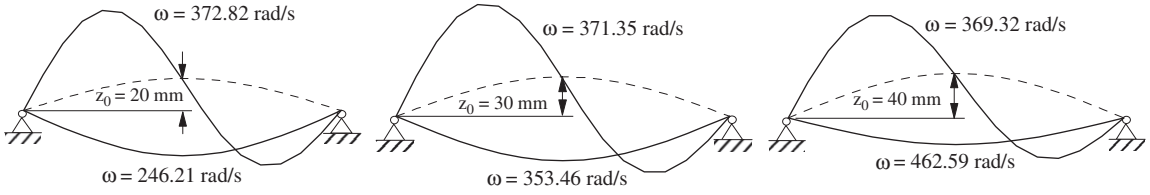

Fig. 18. Arch vibration modes for different z_0 values.

pre-loading on the natural frequencies, but it can also be used, according to the dynamic stability criterion, to identify stable and unstable branches along the equilibrium paths: if $\omega^2 > 0$, the response is stable, while if $\omega^2 < 0$, the response is unstable. Critical conditions are obtained for $\omega^2 = 0$ [49]. This relation has also been proposed as a tool for the experimental identification of critical loads through a non-destructive vibration test using small static pre-loads [6].

Table 1 shows the variation of the first three natural frequencies of the unloaded structure with S_c. For high S_c values, the natural frequencies are well spaced, but when $S_c \to 0$, the joint approaches a perfect hinge, and the first two natural frequencies converge to the same value. Among the analyzed frequencies, the second frequency is influenced more by the connection stiffness than the other two. This can be explained by analyzing the three first vibration modes for $S_c = 0$ (pinned connection), $S_c = 5EI/L$ (semi-rigid connection), and $S_c \to \infty$ (rigid connections) illustrated in Fig. 4. The variation of the angle between the bars with S_c is larger for the second mode, leading to a larger contribution of the spring to the total stiffness of the system.

The static and dynamic post-critical behavior of the loaded L-frame, with beam–column stiffness connection $S_c = 5EI/L$, is illustrated in Figs. 5 and 6. Fig. 5a shows the variation of P/P_e with θ, while Fig. 5b shows the variation of the load with the vertical displacement of the node, w. Fig. 6 shows the variation of the two first natural frequencies with the load up to very large displacements and rotations. Capital letters are used in these figures to identify some reference configurations in both figures. Continuous and dashed curves identify stable and unstable configurations, respectively. The results show that the static pre-load has a strong influence on both frequencies. Knowing that, in the regions of the trajectory where the equilibrium is stable, all the natural frequencies have real values, and that the corresponding regions with negative values of ω^2 are unstable (natural frequency with imaginary value), the stable and unstable equilibrium configurations can be defined, as illustrated in Figs. 5

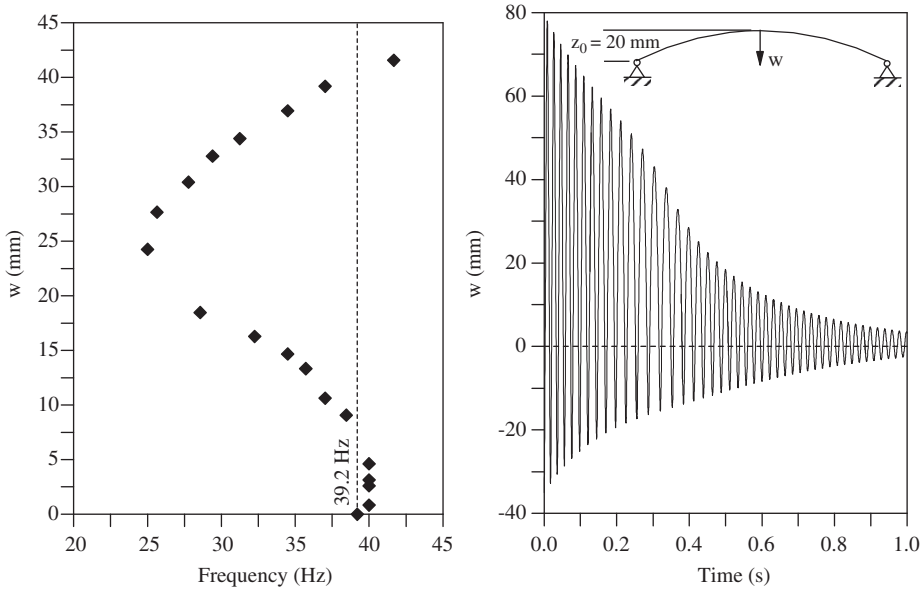

Fig. 20. Frequency–amplitude relation and large amplitude nonlinear time response.

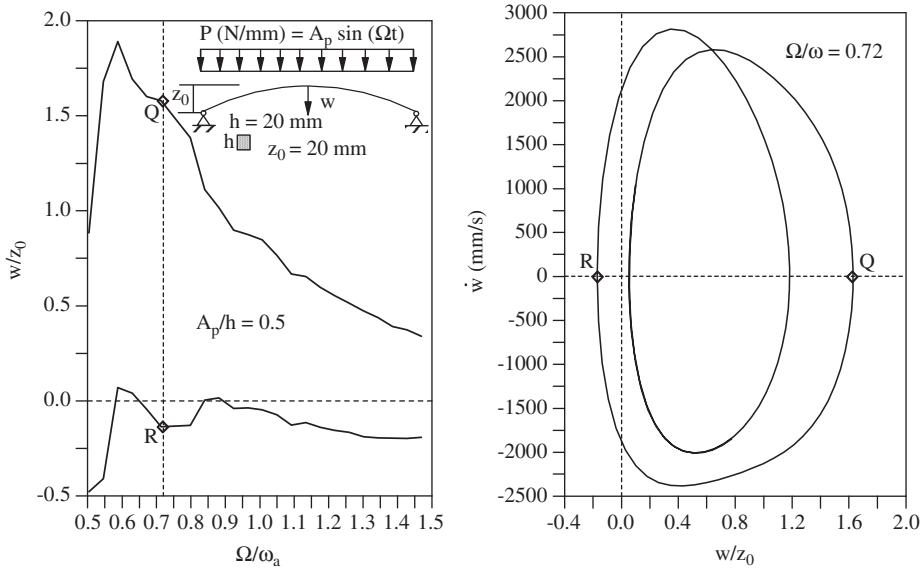

Fig. 21. Resonance analysis: phase diagram with the maximum and minimum amplitudes.

and 6. Through this analysis, various saddle-node bifurcations (fold points) are identified along the post-buckling path. The simultaneous calculation of the nonlinear path and the lowest natural frequencies associated with each equilibrium position has been shown to be a computationally easy and efficient method for the analysis of the stability of the equilibrium paths.

4.1.2. Transient and resonance analysis

Fig. 7 shows the frequency–amplitude relation obtained by the methodology described in Section 3.1 for different values of S_c up to very large deflections. For $S_c=0$, the frame shows a slight softening behavior; for higher values of S_c, the response becomes of the hardening type, showing an increase of the nonlinear frequency with the vibration amplitude. Consider now the same L-frame given in Fig. 1 with a beam–column stiffness connection $S_c=5EI/L$ and a viscous damping matrix proportional to the mass and stiffness matrices, $\boldsymbol{C}=\alpha\boldsymbol{M}+\beta\boldsymbol{K}_t$, defined by Rayleigh coefficients α and β, which are calculated here based on the critical damping coefficient $\xi=0.12$ of the first and second modes. The frame behavior under a suddenly applied step load of infinite duration (Fig. 1a) is analyzed. Fig. 8 shows the transient L-frame response under increasing load levels. The frame exhibits large amplitude vibrations during the transient phase and converges to the static configuration corresponding to the applied load level.

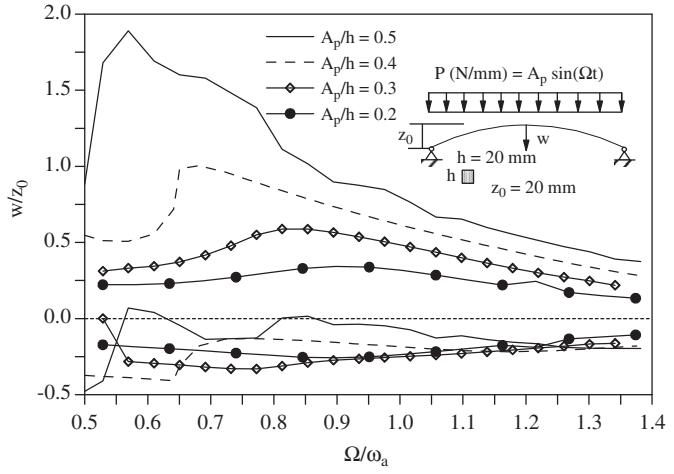

Fig. 22. Arch resonance curves for different amplitudes of the harmonic excitation.

For a harmonic load (Fig. 1b) and using the procedure described in Section 3.1, the resonance curves for the L-frame are obtained considering a perfectly rigid connection between the beam and the column for increasing values of the excitation amplitude, A_p. Fig. 9 exhibits the variation of the amplitude of the steady state solution $|\theta_{max}-\theta_{min}|$ with the frequency ratio Ω/ω_a, where Ω is the excitation frequency of the harmonic load and $\omega_a=\omega_0\sqrt{1-\xi^2}$ is the first natural frequency of the damped frame. The influence of the nonlinearity is small, which is explained by the frequency–amplitude relation shown in Fig. 7. However, as A_p increases, the resonance peak moves to a higher frequency range due to the hardening character of the nonlinearity. The phase planes of the steady-state response for $A_p/P_e=0.4$ and selected values for the excitation frequency are presented in Fig. 10. The asymmetry of the response with respect to θ ($|\theta_{max}|<|\theta_{min}|$) is due to the asymmetric character of the frame nonlinearity, leading to the presence of both quadratic and cubic nonlinearities in the equations of motion.

A similar analysis is performed here considering a distributed harmonic load along the beam. The resonance curves are depicted in Fig. 11. In this case, contrary to the previous one, a marked softening behavior is observed, with the resonant peak moving to the lower frequency range. As shown by Galvão et al. [24], the nonlinear equilibrium path of this frame exhibits a strong nonlinearity associated with a significant loss of initial stiffness. The same influence of this type of load is now observed on the dynamic nonlinear response.

4.2. Shallow arch

The dynamic response of shallow arches has been extensively analyzed due to their practical applications in the various branches of engineering, particularly in large civil engineering structures. Consider an arch with semi-rigid supports submitted to a uniformly distributed vertical load P, as illustrated in Fig. 12.

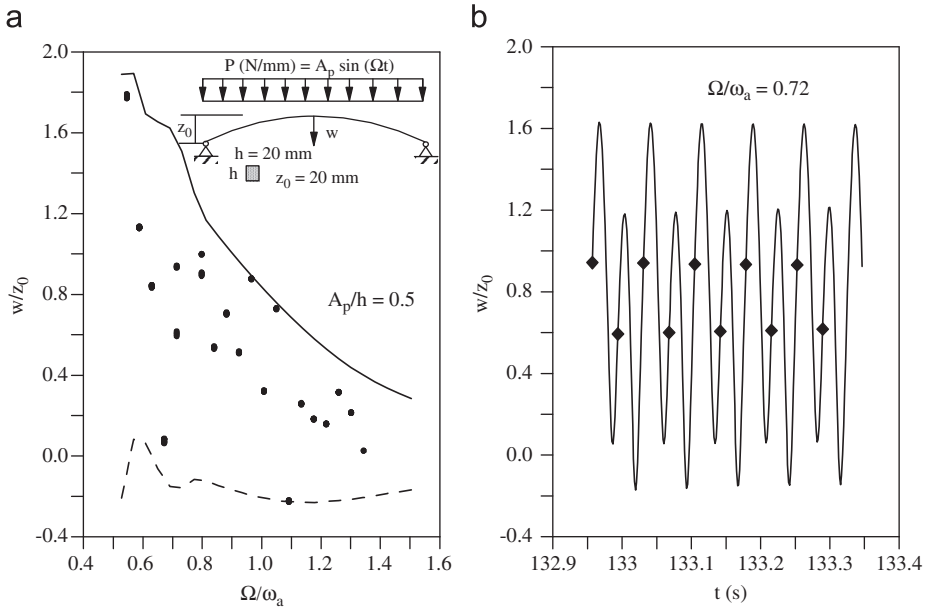

Fig. 23. Period duplication. (a) Poincaré's coordinates and (b) time response solution.

4.2.1. Instability and vibration analysis

Fig. 13 shows the nonlinear equilibrium paths for increasing values of the connection stiffness S_c. For a simply supported arch ($S_c=0$) the present results agree well with those obtained by Bergan [47]. For small values of S_c, two limit points (fold bifurcations) separating the intermediate unstable path from the two stable branches are observed. As S_c increases, the limit points disappear and the arches exhibit highly nonlinear ascending equilibrium paths.

The nonlinear relation between the load and the lowest natural frequency for different values of the connection stiffness is given in Fig. 14. As shown above, this relation not only shows the influence of static pre-loading on the natural frequencies, but can also be used to identify stable and unstable branches along the equilibrium paths according to dynamic stability criteria. In the present analysis, the unstable branches are located between the two limit points of the equilibrium paths (A_1, A_2, B_1, B_2, C_1, and C_2). The literature describes various types of arches, particularly shallow-arches designed for roofs that have lost their stability due to the deterioration of the supports. Corrosion is one of the most frequent causes for the loss of stiffness of the support. In this case, there is a slowly decreasing value for S_c and, consequently, a marked decrease in the overall structure stiffness and dynamic characteristics, as shown herein. These changes can only be evaluated through detailed analysis of the nonlinear structural behavior.

As S_c or the arch height increases, before the load reaches the upper limit point value, the arch may lose stability through an unstable bifurcation, upon which the arch assumes an asymmetric configuration. Figs. 15–17 show the nonlinear equilibrium path of a sinusoidal pinned arch for three values with a height z_0 (20, 30, and 40 mm, respectively) and the variation of the two lowest natural frequencies as a function of the static pre-load. Fig. 18 exhibits the first two vibration modes for the three different values of z_0. For small values of z_0, the first mode is always symmetric, and the second asymmetric, and the two frequencies are well spaced. As the z_0 increases, the frequencies approach each other, and for a critical value of z_0, the frequency associated with the asymmetric frequency mode becomes lower than that of the symmetric mode. This occurs at the point when the structural instability transitions from limit point to unstable bifurcation, since the same nonlinearity that changes the loss of stability mechanism also changes the modal form.

The variation of the first two natural frequencies of the arch as a function of z_0 is illustrated in Fig. 19 for different values of the semi-rigid connection S_c. While the frequency associated with the symmetric mode increases linearly with z_0, the frequency associated with the asymmetric mode remains nearly constant. For $S_c=0$ and $z_0 \cong 31.6$ mm, the first two frequencies are practically coincident. The value of z_0 where this crossing occurs increases with S_c. In structures with accentuated nonlinear behavior, this often occurs and creates various internal resonance phenomena.

4.2.2. Transient and resonance analysis

Fig. 20 shows a typical frequency–amplitude relation for a shallow arch showing the initial softening behavior and the

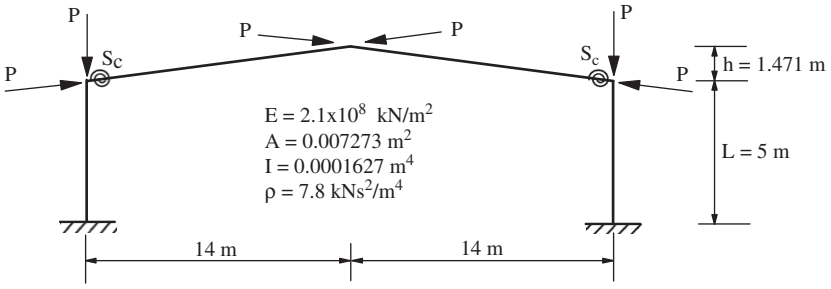

Fig. 24. Pitched-roof steel frame with beam–column flexible joints.

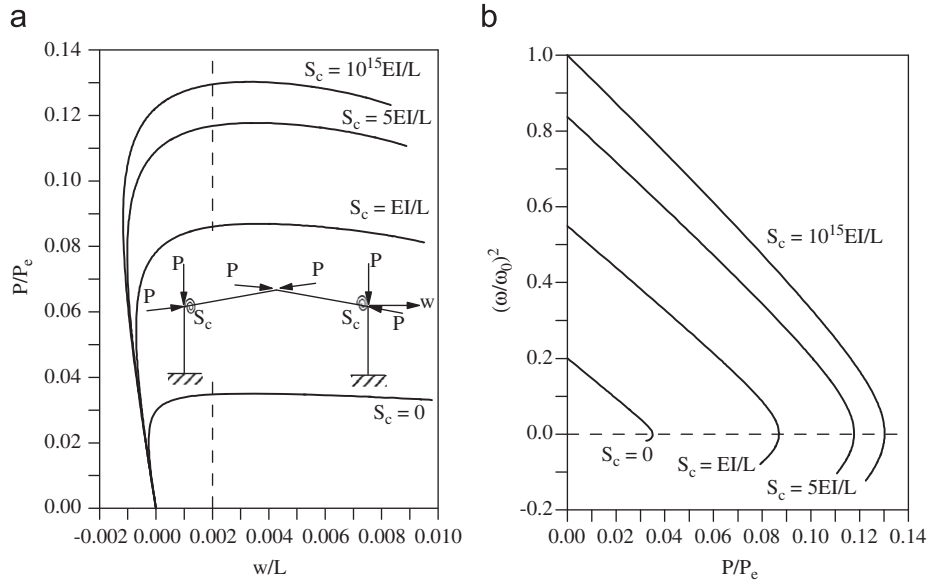

Fig. 25. Influence of the semi-rigid joint stiffness S_c on the nonlinear equilibrium paths and frequency–load relation.

change from softening to hardening at large deflections, due to increasing flexural stiffness. A typical nonlinear time response starting at a highly deformed configuration in the form of the first vibration mode is also shown in Fig. 20, where the nonlinear variation of amplitude with the vibration period is clearly shown.

The dynamic response of the arch under a uniformly distributed harmonic is investigated next. A pinned arch with $z_0=20$ mm is considered. Fig. 21 shows the variation of the maximum and minimum amplitude of the response as a function of the forcing frequency parameter Ω/ω_a for an excitation amplitude relation $A_p/h=0.5$ MPa. $\omega_a=238.4$ rad/s is the lowest natural frequency. Fig. 21 also displays a phase diagram for $\Omega/\omega_a=0.72$.

Fig. 22 illustrates the non-dimensional vertical displacement of the arch mid-span w/z_0 as a function of Ω/ω_a for various values of A_p/h. When the excitation magnitude increases, the resonance peaks move sharply to the lower frequency range, indicating a strong softening behavior in agreement with the frequency–amplitude relation shown in Fig. 20. This behavior is also compatible with the type of nonlinearity observed in the system's static solution. As is typical of nonlinear systems, the resonance curve begins to bend at $A_p/h=0.4$ in a region of low frequencies, which produces more than one permanent solution for the same frequency value. When the magnitude of excitation reaches $A_p/h=0.5$, the amplitude increases considerably in the low frequency region up to the point where the arch loses stability and inverts its concavity. Before this phenomenon occurs, period multiplying bifurcations are observed. A typical solution for this region is shown in Fig. 23a, and its time response is presented in Fig. 23b. The points highlighted in Fig. 23 correspond to the points of the Poincaré section of the steady-state solutions, which clearly indicate the duplication of the period.

4.3. Pitched-roof frame

The numerical strategy developed is now applied to the analysis of a pitched-roof frame with beam–column flexible

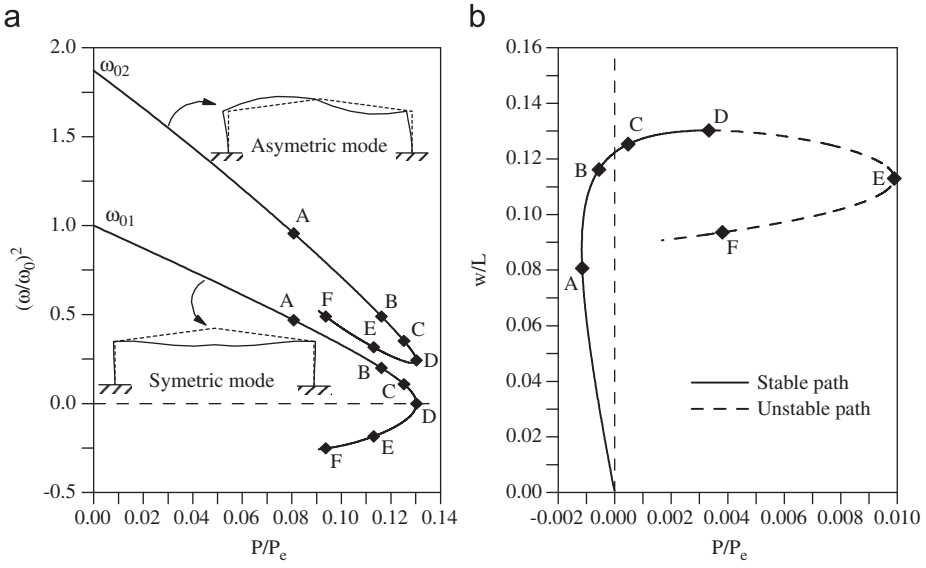

Fig. 26. The pitched-roof frame with beam–column rigid connection. (a) First and second natural frequency–load relation and (b) nonlinear equilibrium path.

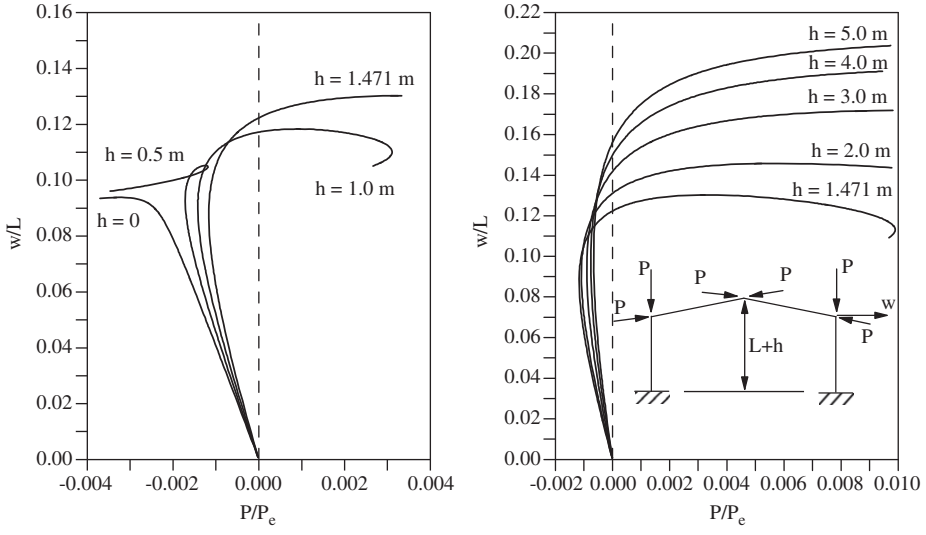

Fig. 27. Variation of the nonlinear equilibrium path with the parameter h.

joints, as shown in Fig. 24. Twenty finite elements are used here to model the structure.

4.3.1. Instability and vibration analysis

Fig. 25a shows the nonlinear equilibrium paths for increasing values of the joint stiffness S_c. The nonlinear relation between the load and the natural frequencies for different values of joint stiffness is given in Fig. 25b. The applied load is non-dimensionalized by $P_e=\pi^2EI/L^2$, and the frequencies are non-dimensionalized by the lowest free vibration frequency of the unloaded frame with rigid connections, $\omega_0=23.912$ rad/s. For the frame with rigid connections, the lowest natural frequency is associated with a symmetric flexural vibration mode, while the second lowest frequency is associated with an asymmetric flexural mode, as shown in Fig. 26, which presents the variation of these two frequencies along the pre- and post-buckling path.

Fig. 27 illustrates the variation of the nonlinear equilibrium path with the geometric parameter h of the pitched-roof frame

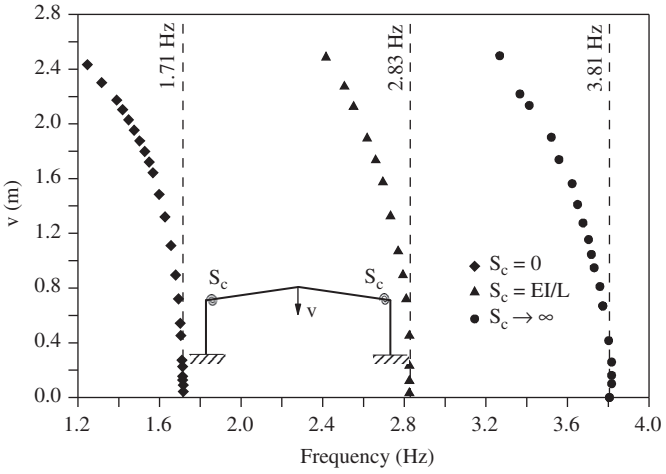

Fig. 29. Nonlinear frequency–amplitude relation for selected values of the connection stiffness S_c.

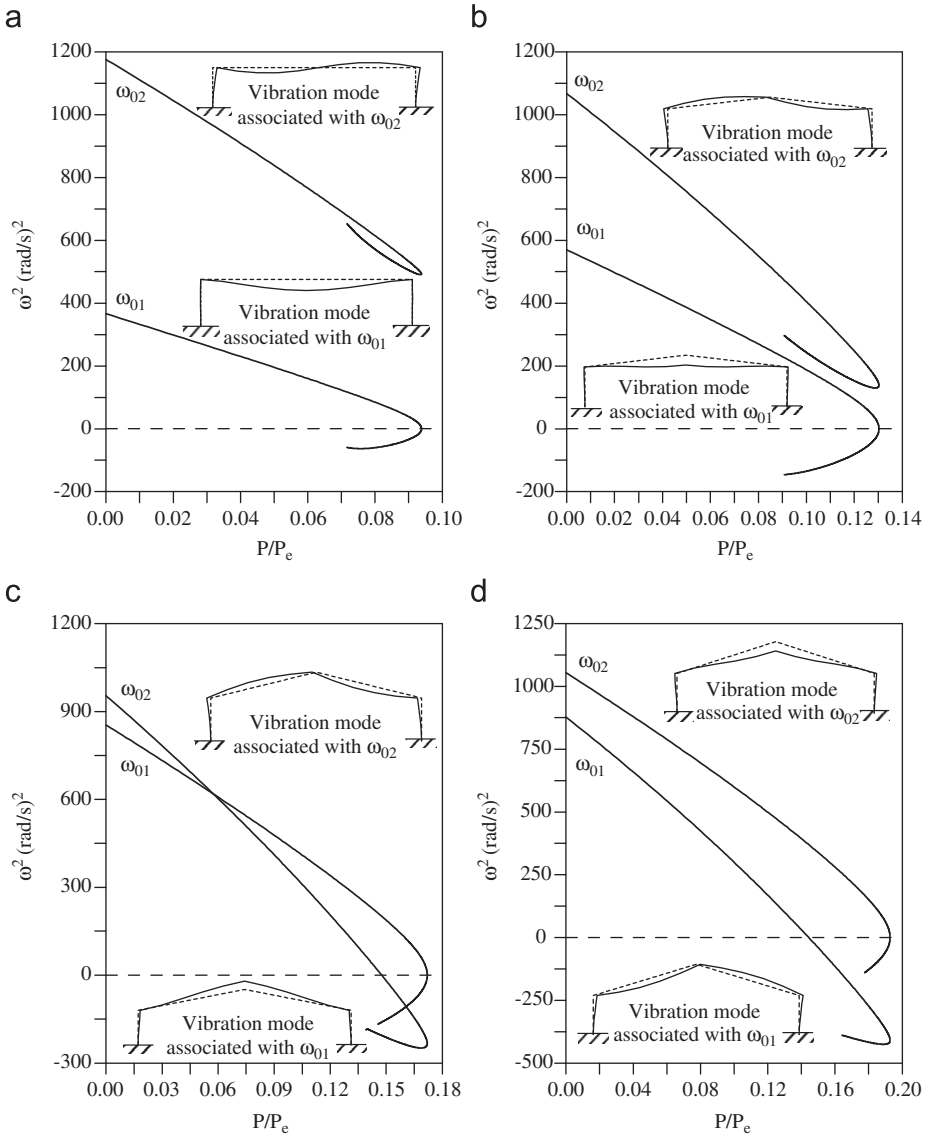

Fig. 28. Variation of the first two natural frequencies (ω_{01} and ω_{02}) and their corresponding vibration modes with the parameter h. (a) $h=0$, (b) $h=1.471$ m, (c) $h=3$ m and (d) $h=4$ m.

(see Fig. 24) and Fig. 28 shows the variation of the two lowest natural frequencies of the frame with the applied load P for selected values of h together with the corresponding free vibration modes. For small values of h, the two lowest frequencies are well separated for any load value. The lowest frequency corresponds to a symmetric flexural mode, while the second frequency corresponds to an asymmetric mode. As the height of the roof increases, the curves corresponding to these modes approach each other and finally intersect, at a certain value of P/P_e (see the results for $h=3$ m), and, after this point, the lowest frequency becomes associated with the asymmetric mode. If h increases still further, the difference between the frequencies increases again, as shown in the figure for $h=4$ m. Again the variation of these frequencies shows that these frames may display various types of internal resonance and exhibit a complex dynamic.

Finally, Fig. 29 shows the frequency–amplitude relation of the pitched-roof for three selected values of the stiffness of the semi-rigid connection. The relation is almost linear for small-to-medium amplitude oscillations of the softening type when very large vibration amplitudes occur, which is outside the range of practical applications.

Although this paper is restricted to the elastic nonlinear behavior of slender frames, one must have in mind that buckling may occur in the elastic range but added stresses due to bending may cause the combined stress to exceed the elastic stress range, or either due to several factors such as residual stresses, initial geometric imperfections and inherent nonlinearity of the stress–strain relationship, the buckling loads may occur in the inelastic range. This occurs in most civil engineering applications and, in such cases, the stability and vibration analysis must be conducted taking into account large deflections and plastification of members and joints with the consequent force redistributions. In this case, the nonlinear dynamic analysis must include the cyclic behavior of the semi-rigid joints [51].

5. Conclusions

The results presented in this paper indicate that the precise evaluation of the connection stiffness, a key point in the design of metal structures, is essential for the calculation of critical conditions. This is particularly important for practical application where damage usually occurs at the connections, decreasing their stiffness and radically changing the nonlinear behavior of the frame.

The results also indicate that the loss of stiffness of a connection during the service life of the structure may significantly affect the structural behavior under both static and dynamic loads. This is in agreement with the literature describing structural failures due to support deterioration. In these cases, there is a slow decrease in the joint stiffness S_c value with accentuated changes in the overall stiffness of the structure and in its dynamic characteristics, which can only be detected and quantified by detailed nonlinear behavior analyses of the structure. The results also show the influence of semi-rigid connections and static pre-loading on the natural frequencies of the analyzed frames. To obtain a better understanding of the instability phenomena of these structures, the nonlinear frequency–amplitude relation is numerically obtained, and the forced vibrations of these structures when submitted to different dynamic loads are analyzed. The methodology used to obtain the resonance curves and frequency–amplitude relation involves the use of computer-intensive and time-consuming procedures. One approach to solve this problem is the use of precise reduced order models or the implementation of efficient continuation techniques for dynamic bifurcation analysis together with the FE method.

Acknowledgments

The authors wish express their gratitude to CAPES and CNPq for the support received in the development of this research. They also thank FAPEMIG and FAPERJ (Minas Gerais and Rio de Janeiro State Foundations) for the financial support. Special thanks go to Harriet Reis for her editorial reviews.

Appendix A

See Table A1.

Table A1
Algorithm for nonlinear static solution and vibration analysis.

1. Input the material and geometric properties of the frame
2. Obtain the reference force vector $\boldsymbol{F_r}$
3. Displacements and load parameter in the actual equilibrium configuration: ${}^t\boldsymbol{u}$, ${}^t\lambda$
4. **INCREMENTAL TANGENT SOLUTION**: $\Delta\lambda^0$ and $\Delta\boldsymbol{u}^0$
   - 4.1. Calculate the tangent stiffness matrix $\boldsymbol{K}_t$
   - 4.2. Solve: $\delta\boldsymbol{u}_r=\boldsymbol{K}_t^{-1}\boldsymbol{F}_r$
   - 4.3. Define $\Delta\lambda^0$ with a determined strategy for the load increment:
     $\Delta\lambda^0=\pm\Delta l/\sqrt{\delta\boldsymbol{u}_r^T\delta\boldsymbol{u}_r+\boldsymbol{F}_r^T\boldsymbol{F}_r}$, Δl: arch-length, Crisfield [26] or,
     $\Delta\lambda^0=\pm{}^1\Delta\lambda^0\sqrt{\left|\left({}^1\delta\boldsymbol{u}_r^{T\,1}\delta\boldsymbol{u}_r\right)/\left({}^t\delta\boldsymbol{u}_r^T\delta\boldsymbol{u}_r\right)\right|}$, Yang and Kuo [43]
   - 4.4. Calculate: $\Delta\boldsymbol{u}^0=\Delta\lambda^0\cdot\delta\boldsymbol{u}_r$
   - 4.5. Update the variables in the new equilibrium configuration $t+\Delta t$
     ${}^{t+\Delta t}\lambda={}^t\lambda+\Delta\lambda^0$ and ${}^{t+\Delta t}\boldsymbol{u}={}^t\boldsymbol{u}+\Delta\boldsymbol{u}^0$
5. **NEWTON–RAPHSON ITERATION FOR $k=1, 2,\ldots, N_i$**
   - 5.1. Calculate the internal forces vector of the current configuration:
     ${}^{t+\Delta t}\boldsymbol{F}_i^{(k-1)}={}^t\boldsymbol{F}+\boldsymbol{K}_t\Delta\boldsymbol{u}^{(k-1)}$
   - 5.2. Calculate the unbalanced forces vector:
     $\boldsymbol{g}^{(k-1)}={}^{t+\Delta t}\lambda^{(k-1)}\boldsymbol{F}_r-{}^{t+\Delta t}\boldsymbol{F}_i^{(k-1)}$
   - 5.3. Verify the convergence: $||\boldsymbol{g}^{(k-1)}||/||\Delta\lambda^{(k-1)}\boldsymbol{F}_r||\le\xi$, with ξ being the tolerance factor
     YES: stop the iteration cycle and go to item 5.8
   - 5.4. Obtain $\delta\lambda^k$ using an iteration strategy:
     $\delta\lambda^k=-(\Delta\boldsymbol{u}^0)^T\delta\boldsymbol{u}_g^k/((\Delta\boldsymbol{u}^0)^T+\Delta\lambda^0\boldsymbol{F}_r^T\boldsymbol{F}_r)$, or,
     $\delta\lambda^k=-{}^t\delta\boldsymbol{u}_r^T\delta\boldsymbol{u}_g^k/\left({}^t\delta\boldsymbol{u}_r^T\delta\boldsymbol{u}_r^k\right)$, Galvão [44]
   - 5.5. Determine: $\delta\boldsymbol{u}^k=\delta\boldsymbol{u}_g^k+\delta\lambda^k\delta\boldsymbol{u}_r^k$, with:
     $\delta\boldsymbol{u}_g^k=-\boldsymbol{K}_t^{-1(k-1)}\boldsymbol{g}^{(k-1)}$ and $\delta\boldsymbol{u}_r^k=\boldsymbol{K}_t^{-1(k-1)}\boldsymbol{F}_r$
   - 5.6. Update the load parameters and the displacement vectors:
     (a) Incrementals: $\Delta\lambda^k=\Delta\lambda^{(k-1)}+\delta\lambda^k$ and $\Delta\boldsymbol{u}^k=\Delta\boldsymbol{u}^{(k-1)}+\delta\boldsymbol{u}^k$
     (b) Totals: ${}^{t+\Delta t}\lambda={}^t\lambda+\Delta\lambda^k$ and ${}^{t+\Delta t}\boldsymbol{u}^k={}^t\boldsymbol{u}+\Delta\boldsymbol{u}^k$
   - 5.7. Return to Step 5
   - 5.8. Determine the natural frequencies and the associated vibrations modes:
     (a) Update the tangent stiffness matrix $\boldsymbol{K}=\boldsymbol{K_L}+\boldsymbol{K}_\tau$ and the mass matrix $\boldsymbol{M}$
     (b) Decompose the $\boldsymbol{M}$ matrix by the Cholesky Method: $\boldsymbol{M}=\boldsymbol{S}^T\boldsymbol{S}$
     (c) Calculate: $\boldsymbol{Q}=\boldsymbol{S}^{-1}$ and determine: $\boldsymbol{A}=\boldsymbol{Q}^T\boldsymbol{K}\boldsymbol{Q}$
     (d) Solve the eigenvalue problem $\boldsymbol{A}\boldsymbol{X}=\lambda\boldsymbol{X}$ by using the Jacob Method [44] obtaining the eigenvalues (ω^2) in the diagonal of matrix $\boldsymbol{A}$ and the eigenvectors (vibration modes) in the columns of matrix $\boldsymbol{X}$.
6. **MAKE A NEW LOAD INCREMENT AND RETURN TO STEP 3**

Table B1
Algorithm for nonlinear dynamic solution.

1. Input the material and geometric properties of the frame
2. Start the initial displacement, velocity and acceleration vectors ${}^{o}\boldsymbol{u}$, ${}^{o}\dot{\boldsymbol{u}}$ and ${}^{o}\ddot{\boldsymbol{u}}$
3. Form the mass matrix $\boldsymbol{M}$
4. **FOR EACH TIME STEP** Δt
   - 4.1. Form the tangent stiffness matrix $\boldsymbol{K}_t$ and the damping matrix $\boldsymbol{C}$
   - 4.2. Using Newmark parameters β and γ, calculate the constants
     $a_0=\frac{1}{\beta\Delta t^2}$, $a_1=\frac{\gamma}{\beta\Delta t}$, $a_2=\frac{1}{\beta\Delta t}$, $a_3=\left(\frac{1}{2\beta\Delta t}-1\right)$, $a_4=\frac{\gamma}{\beta}-1$,
     $a_5=\frac{\Delta t}{2}\left(\frac{\gamma}{\beta}-2\right)$, $a_6=a_0$, $a_7=-a_2$, $a_8=-a_3$,
     $a_9=\Delta t(1-\gamma)$ and $a_{10}=\gamma\Delta t$
   - 4.3. Form the effective stiffness matrix: $\hat{\boldsymbol{K}}=\boldsymbol{K}_t+a_0\boldsymbol{M}+a_1\boldsymbol{C}$
   - 4.4. Form the effective load vector:
     $\hat{\boldsymbol{F}}={}^{t+\Delta t}\lambda\boldsymbol{F}_r+\boldsymbol{M}\left(a_2{}^{t}\dot{\boldsymbol{u}}+a_3{}^{t}\ddot{\boldsymbol{u}}\right)+\boldsymbol{C}\left(a_4{}^{t}\dot{\boldsymbol{u}}+a_5{}^{t}\ddot{\boldsymbol{u}}\right)-{}^{t}\boldsymbol{F}_i$
   - 4.5. Solve for displacement increments: $\hat{\boldsymbol{K}}\Delta\boldsymbol{u}=\hat{\boldsymbol{F}}$
   - 4.6. **ITERATE CYCLE FOR DYNAMIC EQUILIBRIUM:** $k=1, 2,\ldots$
     - i. Evaluate the approximation of the acceleration, velocities and displacements:
       ${}^{t+\Delta t}\ddot{\boldsymbol{u}}^{k}=a_0\Delta\boldsymbol{u}^{k}-a_2{}^{t}\dot{\boldsymbol{u}}-a_3{}^{t}\ddot{\boldsymbol{u}}$
       ${}^{t+\Delta t}\dot{\boldsymbol{u}}^{k}=a_1\Delta\boldsymbol{u}^{k}-a_4{}^{t}\dot{\boldsymbol{u}}-a_5{}^{t}\ddot{\boldsymbol{u}}$
       ${}^{t+\Delta t}\boldsymbol{u}^{k}={}^{t}\boldsymbol{u}+\Delta\boldsymbol{u}^{k}$
     - ii. Update the geometry of the frame
     - iii. Evaluate the internal forces vector:
       ${}^{t+\Delta t}\boldsymbol{F}_i^{k}={}^{t}\boldsymbol{F}_i+\boldsymbol{K}_t\Delta\boldsymbol{u}^{k}$
     - iv. Calculate the residual vector:
       ${}^{t+\Delta t}\boldsymbol{R}^{(k+1)}={}^{t+\Delta t}\lambda\boldsymbol{F}_r-\left(\boldsymbol{M}{}^{t+\Delta t}\ddot{\boldsymbol{u}}^{k}+C{}^{t+\Delta t}\dot{\boldsymbol{u}}^{k}+{}^{t+\Delta t}\boldsymbol{F}_i^{k}\right)$
     - v. Solve for the corrected displacement increments:
       $\hat{\boldsymbol{K}}\delta\boldsymbol{u}^{(k+1)}={}^{t+\Delta t}\boldsymbol{R}^{(k+1)}$
     - vi. Evaluate the corrected displacement increments:
       $\Delta\boldsymbol{u}^{(k+1)}=\Delta\boldsymbol{u}^{k}+\delta\boldsymbol{u}^{(k+1)}$
     - vii. Check the convergence of the iteration process:
       $\frac{|\Delta\boldsymbol{u}^{(k+1)}|}{|{}^{t}\boldsymbol{u}+\Delta\boldsymbol{u}^{(k+1)}|}\le$ *tolerance factor*
       No: Go to 4.6; Yes: Continue
     - viii. Calculate the acceleration, velocities and displacements at time $t+\Delta t$
5. **FOR THE NEXT STEP**
   - 5.1. Evaluate the internal forces vector
   - 5.2. Select a new time step Δt (adaptive strategy) and return to 4

Appendix B

See Table B1.

References

[1] Simitses GJ. Effect of static preloading on the dynamic stability of structures. AIAA Journal 1983;21(8):1174–80.
[2] Simitses GJ. Dynamic stability of suddenly loaded structures. Springer; 1990.
[3] Wu TX, Thompson DJ. The effects of local preload on the foundation stiffness and vertical vibration of railway track. Journal of Sound and Vibration 1999;219(5):881–904.
[4] Machado SP, Cortínez VH. Free vibration of thin-walled composite beams with static initial stresses and deformations. Engineering Structures 2007;29:372–82.
[5] Zeinoddini M, Harding JE, Parke GAR. Dynamic behaviour of axially pre-loaded tubular steel members of offshore structures subjected to impact damage. Ocean Engineering 1999;26(10):963–78.
[6] Gonçalves PB. Axisymmetric vibrations of imperfect shallow spherical caps under pressure loading. Journal of Sound and Vibration 1994;174(2):249–60.
[7] Massonnet Ch. An accurate approximate formula for assessing the vibration frequency of structures axially loaded. International Journal of Mechanical Sciences 1972;14(11):729–34.
[8] Williams FW. Simple buckling and vibration analyses of beam or spring connected structures. Journal of Sound and Vibration 1979;62(4):481–91.
[9] Rosman R. Buckling and vibrations of spatial building structures. Engineering Structures 1981;3(4):194–202.
[10] Leissa AW, Kang J-H. Exact solutions for vibration and buckling of an SS–C–SS–C rectangular plate loaded by linearly varying in-plane stresses. International Journal of Mechanical Sciences 2002;44(9):1925–45.
[11] Ganesan N, Kadoli R. Buckling and dynamic analysis of piezothermoelastic composite cylindrical shell. Composite Structures 2003;59(1):45–60.
[12] Nieh KY, Huang CS, Tseng YP. An analytical solution for in-plane free vibration and stability of loaded elliptic arches. Computers & Structures 81(13):1311–27.
[13] Xu R, Wu Y-F. Free vibration and buckling of composite beams with interlayer slip by two-dimensional theory. Journal of Sound and Vibration 2008; 313(3–5):875–90.
[14] Souza MA. The influence of changing support conditions on the vibration of buckled plates. Thin-Walled Structures 1994;18(2):133–43.
[15] Tada M, Suito A. Static and dynamic post-buckling behavior of truss structures. Engineering Structures 1998;20(4–6):384–9.
[16] Lestari W, Hanagud S. Nonlinear vibration of buckled beams: some exact solutions. International Journal of Solids and Structures 2001;38(26–27): 4741–57.
[17] Boutyour EH, Azrar L, Potier-Ferry M. Vibration of buckled elastic structures with large rotations by an asymptotic numerical method. Computers & Structures 2006;84(3-4):93–101.
[18] Soong TT, Dargush GF. Passive energy dissipation systems in structural engineering. Chichester: John Wiley & Sons; 1997.
[19] Galambos TV. Guide to stability design criteria for metal structures. 5th ed. Wiley; 1998.
[20] Koiter WT. Post-buckling analysis of simple two-bar frame. In: Broberg B, Hult J, Niordson F, editors. Recent progresses in applied mechanics; 1967. p. 337–54.
[21] Roorda J. The instability of imperfect elastic structures, PhD thesis, University College London, England, 1965.
[22] Silvestre N, Camotim D. Coupled global instabilities in pitched-roof frames. In: Camotim D, Dubina D, Rondal J, editors. Proceedings of the third international conference on coupled instabilities in metal structures: CIMS; 2000. p. 475–87.
[23] Silvestre N, Camotim D. Elastic buckling and second-order behaviour of pitched-roof steel frames. Journal of Constructional Steel Research 2007;63(6):804–18.
[24] Galvão AS, Gonçalves PB, Silveira RAM. Post-buckling behavior and imperfection sensitivity of *L*-frames. International Journal of Structural Stability and Dynamics 2005;5:19–38.
[25] Lee SL, Manuel FS, Rossow EC. Large deflection analysis and stability of elastic frames. Journal of Engineering Mechanics Divison ASCE 1968;94:521–47.
[26] Crisfield MA. Nonlinear finite element analysis of solids and structures. John Wiley & Sons; 1991.
[27] Blevins RD. Formulas for natural frequencies and mode shapes. Van Nostrand Reinhold; 1979.
[28] Chen WF, Goto Y, Liew JYR. Stability design of semi rigid frames. John Wiley & Sons; 1996.
[29] Barsan GM, Chiorean CG, Hu K. Computer program for large deflection elasto-plastic analysis of semi-rigid steel frameworks. Computers & Structures 1999;72:699–711.
[30] Kounadis AN, Ecomonou AP. The effects of the joint stiffness and of the constraints on the type of instability of a frame under follower force. Acta Mechanica 1980;36:157–68.
[31] Faella C, Piluso V, Rizzano G. Structural steel semirigid connections. theory, design and software. Boca Raton, FL: CRC Press LLC; 2000.
[32] Kawashima S, Fujimoto T. Vibration analysis of frames with semi-rigid connections. Computers & Structures 1984;19(1–2):85–92.
[33] Chan SL. Vibration and modal analysis of steel frames with semi-rigid connections. Engineering Structures 1994;16(1):25–31.
[34] Sophianopoulos DS. The effect of joint flexibility on the free elastic vibration characteristics of steel plane frames. Journal of Constructional Steel Research 2003;59(8):995–1008.
[35] Shi G, Atluri SN. Static and dynamic analysis of space frames with nonlinear flexible connections. International Journal for Numerical Methods in Engineering 1989;28:2635–50.
[36] Chan SL, Ho GWM. Nonlinear vibration analysis of steel frames with semirigid connections. Journal of Structural Engineering ASCE 1994;120(4): 1075–87.
[37] Chui PPT, Chan SL. Transient response of moment-resistant steel frames with flexible and hysteretic joints frames. Journal Construction Steel Research 1996;39(3):221–43.
[38] Chui PPT, Chan SL. Vibration and deflection characteristics of semi-rigid jointed frames. Engineering Structures 1997;19(12):1001–10.

[39] Chan SL, Chui PPT. Nonlinear static and cyclic analysis of steel frames with semi-rigid connections. Kidlington, UK: Elsevier; 2000.
[40] Sekulovic M, Salatic R, Nefovska M. Dynamic analysis of steel flexible connections. Computers & Structures 2002;80:935–55.
[41] da Silva JGS, de Lima LRO, Vellasco PCG da S, de Andrade SAL, de Castro RA. Nonlinear dynamic analysis of steel portal frames with semi-rigid connections. Engineering Structures 2008;30(9):2566–79.
[42] Alves RV. Instabilidade não-linear elástica de pórticos espaciais, DSc thesis, COPPE-UFRJ, Rio de Janeiro, 1995.
[43] Yang YB, Kuo SB. Theory and analysis of nonlinear framed structures. Prentice Hall; 1994.
[44] Galvão AS. Instabilidade estática e dinâmica de pórticos planos com ligações semi-rígidas, DSc thesis, PUC-Rio, 2004.
[45] Dokanish MA, Subbaraj K. A survey of direct time-integration methods in computational structural dynamics. Computers & Structures 1989;32(6):1371–86.
[46] Jacob BP. Estratégias computacionais para a análise não-linear dinâmica de estruturas complacentes para águas profundas, DSc thesis, COPPE/UFRJ, Rio de Janeiro, 1990.
[47] Bergan PG. Solution algorithms for nonlinear structural problems. Computers & Structures 1980;12:497–509.
[48] Nandakumar K, Chatterjee A. Resonance, parameter estimation, and modal interactions in a strongly nonlinear benchtop oscillator. Nonlinear Dynamics 2005;40:149–67.
[49] Bazant Z, Cedolin L. Stability of Structures. Oxford, UK: Oxford University Press; 1991.
[50] CEN: ENV 1993—Eurocode 3: Design of Steel Structures, Comité Européen de Normalisation, CEN/TC250/SC3, 1993.
[51] Simões R, da Silva LS, Cruz PJS. Cyclic behaviour of end-plate beam-to-column composite joints. Steel & Composite Structures 2001;1(3):355–76.